THE JOURNAL OF PHYSICAL CHEMISTRY LETTERS
A JOURNAL OF THE AMERICAN CHEMICAL SOCIETY

pubs.acs.org/JPCL
Letter

Strong Dependence of Point Defect Properties in Metal Halide Perovskites on Description of van der Waals Interaction

Linjie Deng, Jingyi Ran, Bipeng Wang, Ariadni Boziki, Alexandre Tkatchenko, Jun Jiang,* and Oleg V. Prezhdo*

Cite This: J. Phys. Chem. Lett. 2024, 15, 10465−10472

ABSTRACT: Weaker than ionic and covalent bonding, van der Waals (vdW) interactions can have a significant impact on structure and function of molecules and materials, including stabilities of conformers and phases, chemical reaction pathways, electro-optical response, electron-vibrational dynamics, etc. Metal halide perovskites (MHPs) are widely investigated for their excellent optoelectronic properties, stemming largely from high defect tolerance. Although MHPs are primarily ionic compounds, we demonstrate that vdW interactions contribute ∼5% to the total energy, and that static, dynamics, electronic and optical properties of point defects in MHPs depend significantly on the vdW interaction model used. Focusing on widely studied $CsPbBr_3$ with the common Br vacancy and interstitial defects, we compare the PBE, PBE+D3, PBE+TS, PBE+TS/HI and PBE+MBD-NL models and show that vdW interactions strongly alter the global and local geometric structure, and change the fundamental bandgap, midgap state energies and electron-vibrational coupling. The vdW interaction sensitivity stems from involvement of heavy and highly polarizable chemical elements and the soft MHP structure.

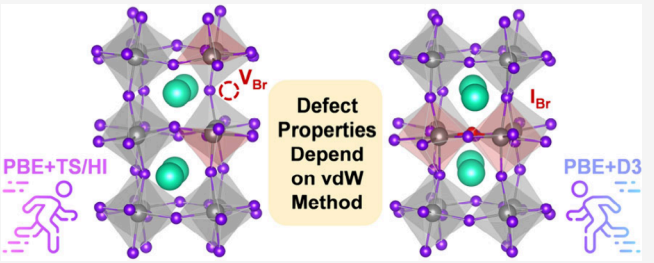

Metal halide perovskites (MHPs) have gathered significant attention for their potential in photovoltaic cells and other applications due to their cost-effective fabrication and high-power conversion efficiency.[1−3] They show exceptional optical properties for solar energy conversion[4] and display promise as semiconductors for efficient,[5] economical transistors,[6] given their ease of processing and high charge carrier mobility. $CsPbBr_3$ is one of the most studied perovskite materials, with applications in high-quality inkjet-printed films for LED technology[7] and quantum information processing.[8] A recent demonstration of phonon-driven intraexciton Rabi oscillations in the orthorhombic phase $CsPbBr_3$ single crystals has opened new avenues for enhancing optoelectronic properties.[9] However, intrinsic defects, such as vacancies, interstitials and antisites, are common and unavoidable in both low-dimensional and 3D bulk materials, influencing their structural and electronic properties, as previously examined through first-principles calculations.[10,11] It is important to employ accurate methods for modeling defects in MHPs. MHPs are soft materials[12] undergoing large-scale structural rearrangements[13] that influence the electronic properties. The static and dynamic structure of MHPs is governed by a delicate interplay of ionic interactions, and covalent and hydrogen bonding.[14,15] Nuclear quantum effects of light hydrogens can influence the geometry of the heavy inorganic lattice,[16] and van der Waals (vdW) interactions play an important role.[17,18]

Density functional theory (DFT) is the mainstream computational tool used extensively in chemical and materials science due to its relatively high predictive ability, general applicability, and computational efficiency.[19−22] The majority of commonly used DFT functionals are designed to describe short-range bonding interactions, and long-range vdW interactions require a special treatment in DFT. VdW interactions are a key ingredient of many systems and processes, including organic, inorganic and biomaterials,[23,24] heterogeneous and electrocatalysis,[25] tribology,[26] protein stability and function,[27,28] etc. VdW interactions are included in DFT calculations as an addition to the exchange-correlation functionals.[29,30] Furthermore, many studies in Tkatchenko's group have shown that vdW interactions play an important role not only in hard solids,[31] but also in point defects[32] and electronic properties.[33] Popular vdW interaction models include D2,[34] D3,[35] Tkatchenko-Scheffler (TS),[36] Tkatchenko-Scheffler with iterative Hirshfeld partitioning (TS/HI),[37] many-body dispersion (MBD),[38] and nonlocal many-body dispersion (MBD-NL).[39] Proposed by Grimme and coworkers,[34,35,40] DFT-D2 and DFT-D3 are the simplest and most commonly used approaches. To mitigate overestimation

Received: August 14, 2024
Revised: October 1, 2024
Accepted: October 7, 2024
Published: October 11, 2024

https://doi.org/10.1021/acs.jpclett.4c02390
J. Phys. Chem. Lett. 2024, 15, 10465−10472

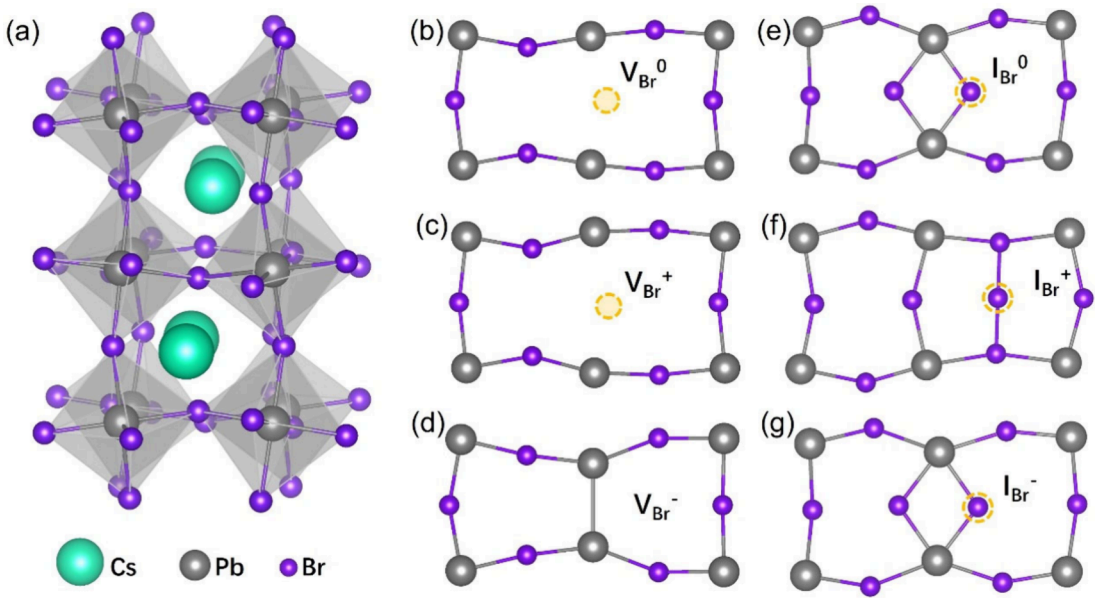

Figure 1. (a) Optimized geometric structure of orthorhombic $CsPbBr_3$. Representation for the optimized atomic structures of (b-d) bromine vacancies and (e-g) bromine interstitials in different charge states. Green, gray, and purple spheres symbolize Cs, Pb, and Br atoms, respectively. Yellow dashed circles specify the vacancies and interstitial atoms. The optimized structures and structural fluctuations at a finite temperature depend significantly on the model for van der Waals interactions.

of vdW interactions in weakly bound systems, DFT-D3 includes a damping function and is often preferred over DFT-D2.[35,41] Tkatchenko and Scheffler developed the TS model, calculating the vdW correction based on the system's ground-state electron density.[36,38] This advanced methodology accounts for environmental and hybridization effects by computing the polarizability of a Hirshfeld volume.[29,42] In order to better characterize the charge transfer, a more advanced TS model using an iterative Hirshfeld allocation scheme (the Hirshfeld-I algorithm)[43,44] was proposed by Bučko et al.[37] While simpler methods consider only pairwise interactions, the MBD method[38] includes collective many-body effects, crucial for accurately describing electronic correlations in larger systems. The MBD method models the interaction between all atoms simultaneously, using a model Hamiltonian based on charged harmonic oscillators that capture the long-range electro-dynamic response. The MBD-NL method[39] extends and refines the original MBD approach[38] to include nonlocal correlation effects.

In this letter, we investigate the significance of an accurate treatment of vdW interactions on structural and electronic properties of MHPs, by computing and comparing the structural parameters and electronic properties of the commonly used bulk $CsPbBr_3$ containing two typical point defects, a Br vacancy (V_{Br}) and a Br interstitial (I_{Br}). We demonstrate that vdW interactions change the properties of bulk $CsPbBr_3$ by 5−7%. The properties of point defects are much more sensitive to the vdW interaction model, because metastable defect structures depend on a delicate balance of various factors and can undergo significant rearrangements and fluctuations. The midgap electronic energy levels in optimized structures and level fluctuations at ambient temperature can vary by nearly 1 eV depending on the description of vdW interactions. The sensitivity stems from the soft nature of MHPs, shallow local energy minima of different MHP structures, and involvement of large, highly polarizable chemical elements. Our findings affirm that an accurate treatment of vdW interactions is essential for studying structural and electronic properties of pristine and particularly defective MHPs.

We focus on the orthorhombic phase of $CsPbBr_3$, the stable phase under ambient conditions.[45−47] The introduction of vdW interactions leads to notable changes in the $CsPbBr_3$ structure and thermodynamic properties. Thermodynamic equations of state (EOS) are used for understanding the behavior of crystalline solids under varying conditions of pressure, volume, entropy, and temperature.[48−50] To determine the lattice constant parameters of the orthorhombic (*Pnma*) $CsPbBr_3$ perovskite unit cell (illustrated in Figure S1a-b, with the unit cell outlined as a frame), the Birch−Murnaghan EOS was employed, in combination with different treatments of vdW interactions for the unit cell optimization. The calculation details are provided in the Supporting Information (SI). The total energy calculated by each method is plotted vs the corresponding calculated volumes, as shown in Figure S1c. The lattice constants and volume of the most stable structure, derived from the EOS fitting, are tabulated in Table S1. This comparison highlights the influence of volume changes on energy: a reduction in energy corresponds to enhanced lattice stability and a decrease in volume, attributable to increased vdW interactions. As expected, incorporating vdW corrections into the PBE framework decreased the equilibrium lattice volume. This is in line with the attractive nature of vdW interactions, which lead to shorter bond lengths in the bulk structure. These findings are in line with previous studies[23,29] which suggest that the attractive nature of vdW interactions typically results in smaller lattice parameters. The PBE+MBD-NL method produced cell parameters in good agreement with the experimental structure of orthorhombic $CsPbBr_3$ measured at 4 K by López et al.,[51] with only a 1% difference in the cell parameters.

Having obtained the optimized unit cells, we construct $CsPbBr_3$ 2×2×2 supercell bulk and introduce the bromine defects, which are the main focus of the study. Additional

https://doi.org/10.1021/acs.jpclett.4c02390
J. Phys. Chem. Lett. 2024, 15, 10465−10472

details about computational methods are provided in the SI. Starting with pristine $CsPbBr_3$, Figure 1a, we introduced the Br vacancy (V_{Br}) and Br interstitial (I_{Br}) defects by removing or adding a Br atom from/to the pristine system. The optimized structures of the defect regions in different charge states are illustrated in Figure 1b-g. The presence of light, external electric field or chemical species can alter the charge of the point defects, and the defect charge can have a strong influence on ionic and electronic conductivity[52,53] and charge carrier lifetime.[54] We consider the positive, neutral and negative charge states for both V_{Br} and I_{Br}. The Pb−Pb distance between the nearest Pb atoms across the defect site is elongated in V_{Br}^{+} compared to V_{Br}^{0}. This change is attributed to the increased repulsion among the Pb^{2+} ions and the positively charged Br vacancy. In contrast, the V_{Br}^{-} system exhibits a reduced Pb−Pb distance, leading to the formation of a Pb dimer. This decrease occurs due to the presence of a negative charge between two Pb^{2+} cations, which draws the neighboring Pb cations closer. Theoretical studies corroborate the formation of stable Pb dimers in the presence of negatively charged halogen vacancies.[55,56] The specific Pb−Pb distances for V_{Br}^{0}, V_{Br}^{+}, and V_{Br}^{-} are detailed in Table 1. The Pb−Pb dimer in the V_{Br}^{-} system remains stable under ambient conditions as well.[56] The variation in the Pb−Pb distances across the Br vacancy obtained with the different vdW interaction models demonstrates a strong impact of vdW interactions on the geometric structure of $CsPbBr_3$. For all charge states of the vacancy defect, the Pb−Pb distance is the greatest when PBE without a vdW correction is used. The Pb−Pb distance decreases when PBE+D3, PBE+TS and PBE+TS/HI are used. The difference between the PBE and PBE+TS results is over 2 Å, indicating that the two methods produce different chemical species. In comparison, the results of PBE+D3 and PBE+TS/HI are close, with variations ranging from 0.03 to 0.18 Å. The additional Br atom in the interstitial system either binds to the two Pb^{2+} cations, Figure 1e,g, or in the positive state forms a Br trimer, Figure 1f. The geometric structure of the Br interstitial system is much less sensitive to the vdW interaction than that of the Br vacancy. The bond distances change only by 0.05−0.1 Å, Table 1. However, even such minor structural changes can lead to notable changes in the electronic energy levels, up to 0.4 eV, Figure S3. The large deformations that occur when using the PBE+TS method may be due to the ionic nature of the material, which is not well handled by the TS correction. However, PBE+TS/HI can handle it better, more accurately than PBE+D3 and without being overcorrected as PBE+TS does.

Table 1. Pb−Pb Distances (Å) across Br Vacancies and Br−Br Distances for Bromine Interstitials Optimized by PBE, PBE+D3, PBE+TS and PBE+TS/HI for the Three Charge States, Figure 1[a]

	Pb−Pb distance for Br vacancy			Br−Br distance for Br interstitial			
method	V_{Br}^{0}	V_{Br}^{+}	V_{Br}^{-}	I_{Br}^{0}	I_{Br}^{+}		I_{Br}^{-}
PBE	5.91	6.43	3.74	3.54	2.567	3.916	3.55
PBE+D3	5.54	6.06	3.69	3.58	2.569	3.933	3.59
PBE+TS	3.85	5.64	3.57	3.55	2.555	3.804	3.60
PBE+TS/HI	5.48	6.24	3.72	3.51	2.554	3.842	3.52

[a]Two distances are given for the I_{Br}^{+} system: the average distances from the interstitial to the nearest top/bottom Br atoms (shorter distance) and to the left/right Br atoms (longer distance), as illustrated in Figure 1f.

Figure 2 presents a total energy comparison for the V_{Br} and I_{Br} systems. The comparison highlights the impact of vdW interactions on the total energies of these systems. Notably, vdW interactions universally stabilize all systems by reducing their total energy. Among the vdW interaction models examined, the TS description produce the greatest variations from the PBE model, followed by the D3 vdW correction and the TS/HI scheme. Overall, vdW interactions contribute about 5% to the total energy. However, even this relatively minor contribution can have a significant influence on the geometric structure and electronic properties of point defects, because MHPs are soft and respond strongly to perturbations.[12,57,58] Comparing the different charge states of the defects, vdW interactions are slightly stronger for the more positive charges, even though the number of electrons is smaller, and vdW interactions generally increase with the number of electrons. Further, the weaker vdW interaction in the negatively charged V_{Br}^{-} system causes more significant changes in the geometric properties compared to the neutral and positive vacancies, Figure 1 and Table 1.

To elucidate the impact of vdW interactions models on the electronic properties of the $CsPbBr_3$ systems with point defects, we calculated the density of states (DOS) and the electronic band structure on both defective and pristine structures, as depicted in Figures 3 and S2−4. The results indicate that vdW interactions can notably affect the fundamental bandgaps and midgap states. Figure 3 illustrates the total DOS for all systems with a Br vacancy, evaluated with the four methods in the corresponding optimized geometries.

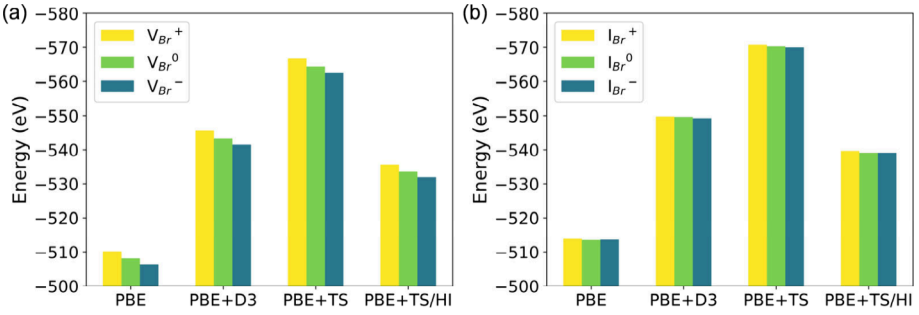

Figure 2. Total energies of (a) Br vacancy and (b) Br interstitial systems in different charge states, calculated using PBE, PBE+D3, PBE+TS and PBE+TS/HI. VdW interactions models contribute 5−10% to the total energy, with the TS model making a notably larger contribution than the D3 and TS/HI models. The charge has a stronger effect on the total energy of the vacancy than the interstitial.

https://doi.org/10.1021/acs.jpclett.4c02390
J. Phys. Chem. Lett. 2024, 15, 10465−10472

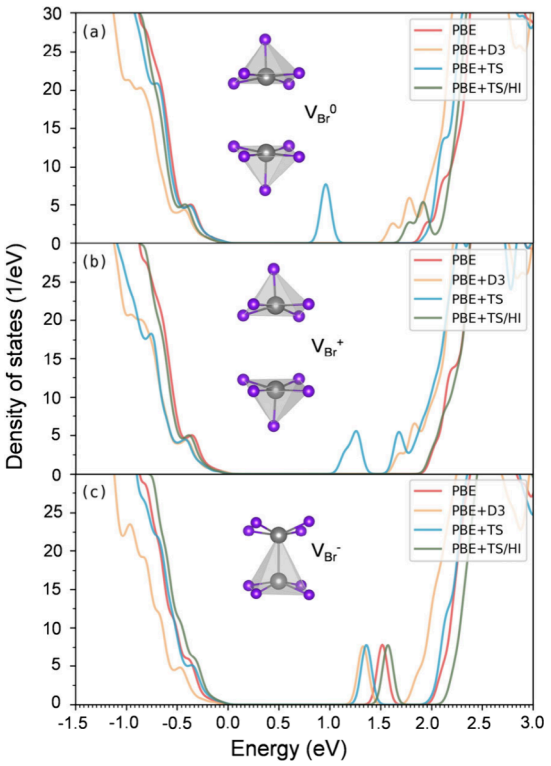

Figure 3. Electronic density of states of $CsPbBr_3$ with (a) neutral, (b) positive, and (c) negative Br vacancy in the optimized geometries, calculated using PBE, PBE+D3, PBE+TS and PBE+TS/HI. The zero energy is set to the VBM. The insets depict structures of the Br vacancy in the respective charge states. Gray, and purple spheres represent Pb and Br atoms, respectively. Distinctly, a midgap trap state appears in both V_{Br}^0 and V_{Br}^+ systems at the PBE+TS level, but not the other three methods. Additionally, the fundamental bandgaps are sensitive to the van der Waals interaction model.

For V_{Br}^0, Figure 3a, the PBE+TS model predicts a prominent midgap trap state located 0.8 eV below the conduction band minimum (CBM). In the case of V_{Br}^+, Figure 3b, the midgap trap state in the PBE+TS model shifts closer to the CBM, and an additional peak appears near the band edge. In contrast, the PBE+D3 model predicts shallow trap states for both V_{Br}^0 and V_{Br}^+, whereas the PBE+TS/HI model predicts only shallow trap states for V_{Br}^0. In V_{Br}^- (Figure 3c), midgap trap states are identified with all four calculations, a phenomenon that can be attributed to the formation of a dimer between the two Pb atoms across the vacancy.

The DOS results for bulk pristine $CsPbBr_3$ and the I_{Br} systems, Figures S3 and S4, exhibit a weaker dependence on the vdW interaction model, while the trends are similar. The band gap is the lowest in the PBE+D3 method. Only the I_{Br}^+ defect demonstrates midgap trap states at energies that depend on the vdW interaction model, Figure S3b, suggesting that the trap state originates due to electrostatic and covalent interactions resulting in formation of the I_3 trimer, Figure 1f. At the same time, the energy of the trap state varies 0.5 eV depending on the description of the vdW interaction.

The band structure calculations further substantiate the fact that vdW interactions models have a pronounced impact on the electronic properties of the point defects in $CsPbBr_3$. Focusing only on the neutral defects, Figure S4 demonstrates that the valence band maximum (VBM) and CBM are mainly contributed by Pb and Br atoms, respectively. V_{Br}^0 exhibits an unoccupied midgap state, whose energy depends strongly on the vdW interaction model. Notably, the midgap state exhibits no dependence on the k-point in the PBE+TS calculation, indicating that it is a localized state. In contrast, the PBE, PBE+D3 and PBE+TS/HI methods show k-point dependence of the trap state energy between the R and G points. Dependence arises, because the midgap state, which is close to the CBM, mixes with the band states, and is partially delocalized. The electrons trapped by the shallow midgap states predicted by PBE, PBE+D3 and PBE+TS/HI can easily escape into the band. In comparison, the trap state obtained by PBE+TS is 1 eV below the CBM. The depth is much larger than the thermal energy, equal to 25 meV at room temperature, suggesting that the midgap state can trap charge carriers permanently, accelerating nonradiative recombination.[59] This finding confirms earlier computational analyses by Kang et al. and Shi et al.[10,60]

Most MHPs, including $CsPbBr_3$, are soft and susceptible to significant structural fluctuations at a finite temperature. These fluctuations particularly influence electronic energy levels associated with defects, often resulting in an unusual behavior.[61,62] To study the influence of the vdW interaction model on fluctuations of the defect energy levels we conducted ab initio molecular dynamics (MD) simulations for the V_{Br}^0 and I_{Br}^0 systems, Figures 4 and S5−S6. In V_{Br}^0, midgap trap

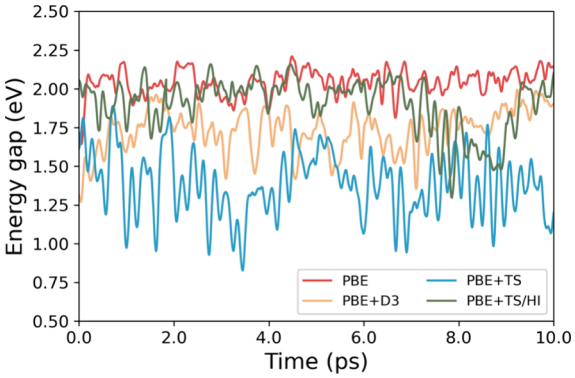

Figure 4. Fluctuation of the midgap state energy relative to HOMO in $CsPbBr_3$ with a neutral Br vacancy, calculated using PBE, PBE+D3 and PBE+TS along the 10 ps MD trajectories at 300 K. Stronger vdW interactions both lower the trap state energy and increase its fluctuation.

states emerge from Pb−Pb interactions during structural oscillations. These midgap states, originating from the separation of the lowest unoccupied molecular orbital (LUMO) and highest occupied molecular orbital (HOMO) from the conduction and valence bands, trap charge carriers, thereby affecting their transport and recombination.[12,54,63] The presence of deep midgap trap states is highlighted by prolonged structural distortions. The occurrence of midgap states induced by a halide vacancy defect is closely linked to the Pb−Pb distances between the adjacent Pb atoms and ion coordination numbers during fluctuations.[13,62] Figure S5 presents the energy levels from HOMO−2 to LUMO+2 as functions of time along the MD trajectory for $CsPbBr_3$ with V_{Br} and I_{Br}. Midgap states are consistently observed in all V_{Br} systems, Figure S5a-d, but not in the I_{Br} systems, Figure S5e-h, similar to the previous findings.[61,64] For models predicting stronger vdW interactions, the defect states in $CsPbBr_3$ with a Br vacancy become deeper, and the amplitude of their energy

https://doi.org/10.1021/acs.jpclett.4c02390
J. Phys. Chem. Lett. 2024, 15, 10465−10472

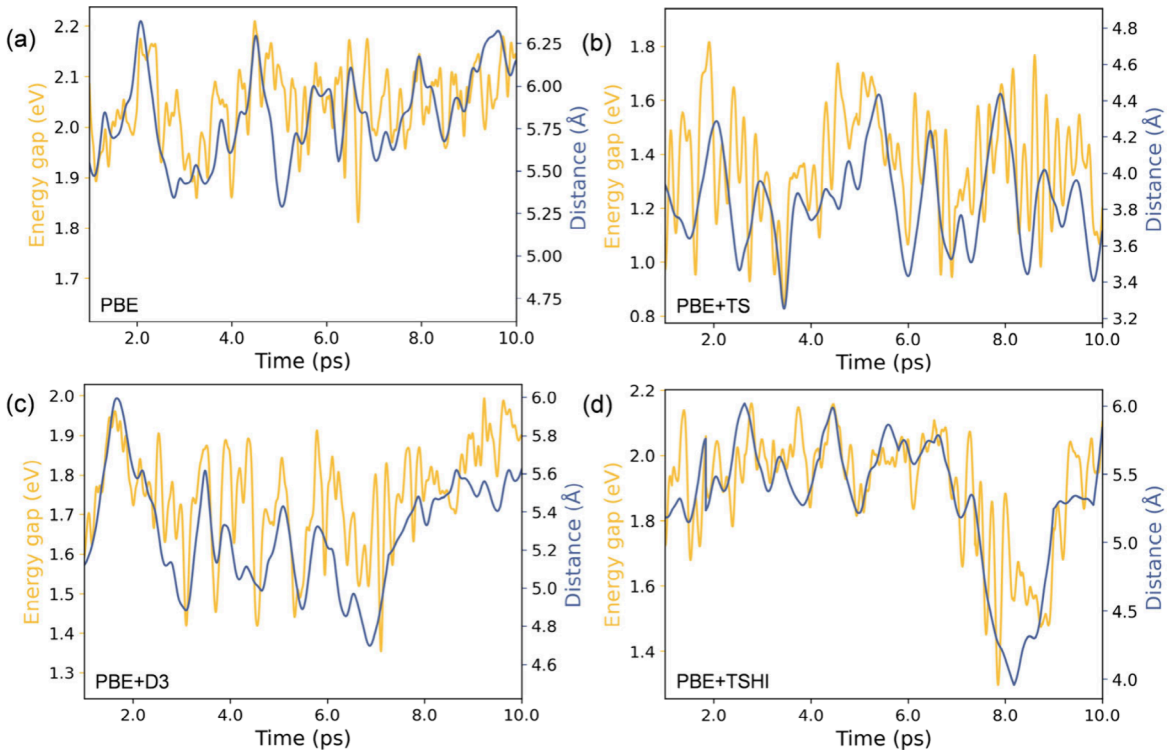

Figure 5. Relationship between the midgap state energy and the Pb−Pb distance across the Br vacancy calculated with (a) PBE, (b) PBE+D3, (c) PBE+TS and (d) PBE+TS/HI. In all methods, a clear correlation exists between the energy gap and the Pb−Pb distance.

fluctuation increases, Figure S5b-c. Figure S6 presents distributions of the vacancy trap energies obtained by the four methods. Under the influence of vdW interactions, the energy distribution becomes broader, indicating enhanced fluctuations. The corresponding standard deviations change from 0.08 to 0.14 eV to 0.20 eV and to 0.17 eV in the PBE, PBE+D3, PBE+TS and PBE+TS/HI calculations. Figure 4 compares the evolution of the energy gap between the defect state and HOMO for the V_{Br}^{0} system in $CsPbBr_3$ bulk obtained with the PBE, PBE+D3, PBE+TS and PBE+TS/HI methodologies. This energy gap reduces and its oscillation intensifies for models predicting stronger vdW interactions. The maximum detected energy gap between the HOMO and the midgap state increases from 0.57 eV in PBE to 0.72 eV in PBE+D3 to 1.06 eV in PBE+TS, while it is 0.86 eV in PBE +TS/HI.

In all four methods, the Pb−Pb distances across the vacancy in the V_{Br}^{0} system of $CsPbBr_3$ show a clear correlation with the midgap trap state energy, Figure 5. Cohen et al.[11] previously identified that the depth of the trap state has an inverse relationship with the Pb−Pb distance across the Br vacancy in $CsPbBr_3$. Our calculations corroborate this finding, revealing a strong correlation between the trap state energy and the Pb−Pb distance: the shorter the Pb−Pb distance, the deeper the trap state. The Pb−Pb distance fluctuates from 4.70 to 6.38 Å in the PBE calculation without a vdW correction, and the trap state energy fluctuates between 2.19 and 1.69 eV, Figure S5a. When the D3 vdW correction is included, the distance becomes shorter, fluctuating from 4.49 to 5.99 Å, and the trap state energy levels vary from 1.95 to 1.26 eV, Figure S5b. The Pb−Pb distance decreases further in the PBE+TS calculation, ranging from 3.25 to 4.83 Å, and the trap state becomes deeper, with the energy level fluctuating between 1.88 and 0.84 eV, Figure S5c. However, after the TS/HI vdW correction, the Pb−Pb spacing increases from 3.96 to 6.02 Å, and the energy range of the trap state changes from 2.15 to 1.34 eV, Figure S5d.

Figure 6 displays the charge density associated with the V_{Br}^{0} defect state, as calculated by four methods. The corresponding

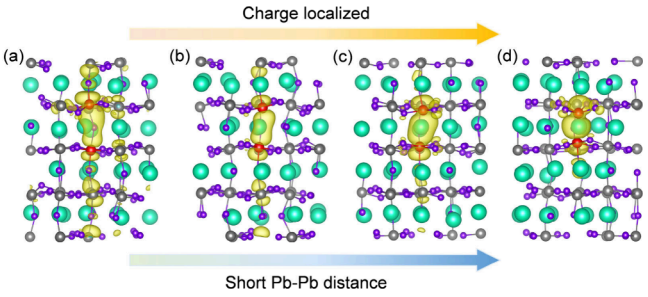

Figure 6. Charge densities of the defect state for a representative structure (at 5 ps) of $CsPbBr_3$ with a neutral Br vacancy, calculated with the (a) PBE, (b) PBE+TS/HI, (c) PBE+D3 and (d) PBE+TS methods. The two Pb atoms across the vacancy are highlighted in red. In contrast to the delocalized VBM and CBM, Figure S7, the defect state is localized at the vacancy. As the Pb−Pb distance shortens, the charge density becomes more localized.

VBM and CBM charge densities are shown in Figure S7. The LUMO charge density is localized around the Br vacancy, as it represents the defect state, while the VBM and CBM charge densities remain delocalized. The PBE+TS method demonstrates significantly more localized charge density around the vacancy compared to the other three vdW models. This increased localization correlates with the shorter Pb−Pb distance and the lower defect level energy discussed above. The charge densities of the V_{Br}^{0} defect state calculated with

https://doi.org/10.1021/acs.jpclett.4c02390
J. Phys. Chem. Lett. 2024, 15, 10465−10472

PBE, PBE+TS/HI and PBE+D3 delocalize partially in the Pb−Pb direction, Figure 5a-c.

Fourier transforms (FTs) of defect energy fluctuations characterize electron-vibrational interactions, Figure 7. The

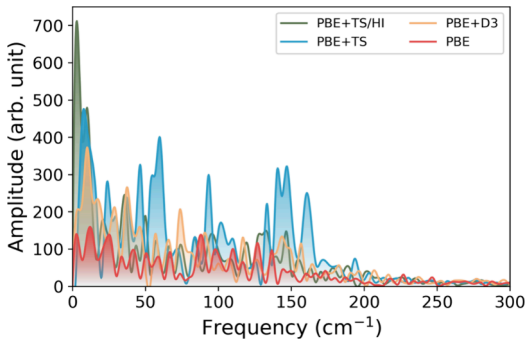

Figure 7. Fourier transforms of fluctuations of the V_{Br}^{0} defect state energy over the 10 ps MD trajectories obtained with the different vdW interaction models. The fluctuations predominantly occur at frequencies of 200 cm^{-1} or lower, and the signal amplitude increases for models predicting stronger vdW interactions, in agreement with Figure 4. The signals associated with the Br vacancy, shown here, are significantly stronger than those for the Br interstitial, Figure S8.

frequencies detected in the FT spectra identify the phonon modes that couple to the electronic subsystem, and the amplitude of the signal at a particular frequency indicates the strength of the electron−phonon coupling for that phonon.[12,64,65] MHPs are composed of heavy elements and are soft.[12,63] As a result, the spectra are dominated by low-frequency signal, below 200 cm^{-1}, Figure 7. The FT amplitudes increase as the frequency decreases, with the strongest peaks seen at 10 cm^{-1} except PBE+TS/HI method. With TS/HI correction, the strongest peak appeared around 3 cm^{-1}, and the amplitude of the second strongest peak is almost the same as that of the strongest peak in the PBE+TS method. Above 10 cm^{-1}, the electron-vibrational coupling is the strongest for PBE+TS, intermediate for PBE+D3 and PBE +TS/HI, and weakest for PBE. Interestingly, the weak signals above 200 cm^{-1} are comparable across the four methods. The FTs indicate that vdW interactions strongly enhance electron-vibrational interactions in MHPs. This is also true for the I_{Br} system, Figure S8. Similar to $CsPbBr_3$ with a Br vacancy, the FT signal amplitudes are higher at lower frequencies, and they intensify for models predicting stronger vdW interactions. However, in the absence of deep midgap trap states in the Br interstitial systems, the FT signals in the low-frequency regions are considerably weaker compared to those in $CsPbBr_3$ containing a Br vacancy. The data shows that the strength of electron-vibrational interactions in MHPs can depend significantly on the vdW interaction model used. Further analysis is needed to establish the sensitivity of elastic and inelastic electron-vibrational scattering on the vdW interaction model.

In summary, we have investigated the influence of the vdW interaction models on structural and electronic properties and electron-vibrational interactions in $CsPbBr_3$ bulk with the halide vacancy V_{Br} and interstitial I_{Br} point defects in negative, neutral and positive charge states. We have compared the results obtained with the commonly used PBE functional without a vdW correction, with the commonly used D3 vdW correction, the TS vdW interaction model and the more advanced TS/HI vdW scheme. Inclusion of vdW interactions notably reduces the $CsPbBr_3$ volume and lowers its energy by 5−7%. The fundamental bandgap changes by a similar amount. The energies of the midgap electronic states arising from structural defects depend much more significantly on the vdW interaction model, because defect structures are less stable than pristine bulk and are more sensitive to the delicate balance of ionic, covalent and vdW forces. The energy of the I_{Br} interstitial level changes by 0.4 eV in the optimized geometry depending on the vdW model. The V_{Br} vacancy is particularly sensitive to vdW interaction model, because of the large, created void that allows significant local structural deformations. The V_{Br} energy level can shift by 1 eV depending on the vdW interaction model and fluctuate by about the same amount at ambient temperature. VdW forces can enhance the strength of electron-vibrational interactions 3-fold. In practice, the TS model may possibly overestimate vdW interactions in MHPs, and the TS/HI model is preferred to the D3 and TS models, even though it is more computationally demanding. The insights gained from this research underscore the significance of accurate treatment of vdW in MHPs and other nanoscale systems, whose structure and electronic properties depend on a delicate balance of many factors.

■ ASSOCIATED CONTENT

Supporting Information

The Supporting Information is available free of charge at https://pubs.acs.org/doi/10.1021/acs.jpclett.4c02390.

Simulation details, unit cell volumes and densities of states of pristine $CsPbBr_3$, densities of states of the Br interstitial system, band structure of pristine and defective $CsPbBr_3$, evolution of band and defect state energies along trajectories, canonical distributions of Br vacancy defect state energies, charge densities of the band edge states of the Br vacancy system, and influence spectra for the Br interstitial system (PDF)

Coordinates of optimized structures (ZIP)

■ AUTHOR INFORMATION

Corresponding Authors

Jun Jiang − *Key Laboratory of Precision and Intelligent Chemistry, Hefei National Research Center for Physical Sciences at the Microscale, School of Chemistry and Materials Science, University of Science and Technology of China, Hefei, Anhui 230026, China;* orcid.org/0000-0002-6116-5605; Email: jiangj1@ustc.edu.cn

Oleg V. Prezhdo − *Department of Chemistry and Department of Physics and Astronomy, University of Southern California, Los Angeles, California 90089, United States;* orcid.org/0000-0002-5140-7500; Email: prezhdo@usc.edu

Authors

Linjie Deng − *School of Chemistry and Materials Science, University of Science and Technology of China, Hefei, Anhui 230026, China*

Jingyi Ran − *Department of Chemistry, University of Southern California, Los Angeles, California 90089, United States;* orcid.org/0000-0003-0579-7138

Bipeng Wang − *Department of Chemical Engineering, University of Southern California, Los Angeles, California 90089, United States;* orcid.org/0000-0003-0924-5867

https://doi.org/10.1021/acs.jpclett.4c02390
J. Phys. Chem. Lett. 2024, 15, 10465−10472

Ariadni Boziki − *Department of Physics and Materials Science, University of Luxembourg, L-1511 Luxembourg City, Luxembourg;* orcid.org/0000-0002-2347-8993

Alexandre Tkatchenko − *Department of Physics and Materials Science, University of Luxembourg, L-1511 Luxembourg City, Luxembourg;* orcid.org/0000-0002-1012-4854

Complete contact information is available at: https://pubs.acs.org/10.1021/acs.jpclett.4c02390

Notes

The authors declare no competing financial interest.

■ ACKNOWLEDGMENTS

L. D. was financially supported by the China Scholarship Council. O. V. P. acknowledges the support of the US National Science Foundation, grant CHE-2154367.

■ REFERENCES

(1) Ezzeldien, M.; Al-Qaisi, S.; Alrowaili, Z. A.; Alzaid, M.; Maskar, E.; Es-Smairi, A.; Vu, T. V.; Rai, D. P. Electronic and Optical Properties of Bulk and Surface of $CsPbBr_3$ Inorganic Halide Perovskite a first principles DFT 1/2 approach. *Sci. Rep.* **2021**, *11*, 20622.

(2) Maafa, I. M. All-Inorganic Perovskite Solar Cells: Recent Advancements and Challenges. *Nanomaterials* **2022**, *12*, 1651.

(3) Mishra, L.; Behera, R. K.; Panigrahi, A.; Sarangi, M. K. Förster Resonance Energy Transfer Assisted Enhancement in Optoelectronic Properties of Metal Halide Perovskite Nanocrystals. *J. Phys. Chem. Lett.* **2022**, *13*, 4357−4364.

(4) Hoang, M. T.; Yang, Y.; Tuten, B.; Wang, H. Are Metal Halide Perovskite Solar Cells Ready for Space Applications? *J. Phys. Chem. Lett.* **2022**, *13*, 2908−2920.

(5) Xia, C. Q.; Peng, J.; Poncé, S.; Patel, J. B.; Wright, A. D.; Crothers, T. W.; Uller Rothmann, M.; Borchert, J.; Milot, R. L.; Kraus, H.; Lin, Q.; Giustino, F.; Herz, L. M.; Johnston, M. B. Limits to Electrical Mobility in Lead-Halide Perovskite Semiconductors. *J. Phys. Chem. Lett.* **2021**, *12*, 3607−3617.

(6) He, Y.; Hadar, I.; Kanatzidis, M. G. Detecting Lonizing Radiation Using Halide Perovskite Semiconductors Processed Through solution and alternative methods. *Nat. Photonics* **2022**, *16*, 14−26.

(7) Vescio, G.; Frieiro, J. L.; Gualdrón-Reyes, A. F.; Hernández, S.; Mora-Seró, I.; Garrido, B.; Cirera, A. High Quality Inkjet Printed-Emissive Nanocrystalline Perovskite $CsPbBr_3$ Layers for Color Conversion Layer and LEDs Applications. *Adv. Mater. Technol.* **2022**, *7*, 2101525.

(8) Crane, M. J.; Jacoby, L. M.; Cohen, T. A.; Huang, Y.; Luscombe, C. K.; Gamelin, D. R. Coherent Spin Precession and Lifetime-Limited Spin Dephasing in $CsPbBr_3$ Perovskite Nanocrystals. *Nano Lett.* **2020**, *20*, 8626−8633.

(9) Nguyen, X. T.; Winte, K.; Timmer, D.; Rakita, Y.; Ceratti, D. R.; Aharon, S.; Ramzan, M. S.; Cocchi, C.; Lorke, M.; Jahnke, F.; Cahen, D.; Lienau, C.; De Sio, A. Phonon-driven Intra-exciton Rabi Oscillations in $CsPbBr_3$ Halide Perovskites. *Nat. Commun.* **2023**, *14*, 1047.

(10) Kang, J.; Wang, L. W. High Defect Tolerance in Lead Halide Perovskite $CsPbBr_3$. *J. Phys. Chem. Lett.* **2017**, *8*, 489−493.

(11) Cohen, A. V.; Egger, D. A.; Rappe, A. M.; Kronik, L. Breakdown of the Static Picture of Defect Energetics in Halide Perovskites: The Case of the Br Vacancy in $CsPbBr_3$. *J. Phys. Chem. Lett.* **2019**, *10*, 4490−4498.

(12) Chu, W.; Saidi, W. A.; Zhao, J.; Prezhdo, O. V. Soft Lattice and Defect Covalency Rationalize Tolerance of β-$CsPbI_3$ Perovskite Solar Cells to Native Defects. *Angew. Chem., Int. Ed.* **2020**, *59*, 6435−6441.

(13) Liu, D.; Wu, Y.; Vasenko, A. S.; Prezhdo, O. V. Grain Boundary Sliding and Distortion on a Nanosecond Timescale Induce Trap States in $CsPbBr_3$: Ab Initio Investigation with Machine Learning Force Field. *Nanoscale* **2022**, *15*, 285−293.

(14) Qiao, L.; Fang, W. H.; Long, R.; Prezhdo, O. V. Photoinduced Dynamics of Charge Carriers in Metal Halide Perovskites from an Atomistic Perspective. *J. Phys. Chem. Lett.* **2020**, *11*, 7066−7082.

(15) Ambrosio, F.; De Angelis, F.; Goni, A. R. The Ferroelectric-Ferroelastic Debate about Metal Halide Perovskites. *J. Phys. Chem. Lett.* **2022**, *13*, 7731−7740.

(16) Liu, Y.; Long, R.; Fang, W. H.; Prezhdo, O. V. Nuclear Quantum Effects Prolong Charge Carrier Lifetimes in Hybrid Organic-Inorganic Perovskites. *J. Am. Chem. Soc.* **2023**, *145*, 14112−14123.

(17) Wang, Q.; Niu, X.; Ning, W.; Zhu, Z.; Shi, R.; Zhao, Y. Interaction of organic-inorganic hybrid perovskite electron system with lattice system. *Mater. Today Sustainability* **2024**, *25*, 100617.

(18) Varadwaj, P. R.; Varadwaj, A.; Marques, H. M.; Yamashita, K. Significance of hydrogen bonding and other noncovalent interactions in determining octahedral tilting in the $CH_3NH_3PbI_3$ hybrid organic-inorganic halide perovskite solar cell semiconductor. *Sci. Rep.* **2019**, *9*, 50.

(19) Araujo, R. B.; Rodrigues, G. L. S.; Dos Santos, E. C.; Pettersson, L. G. M. Adsorption Energies on Transition Metal Surfaces: Towards an Accurate and Balanced Description. *Nat. Commun.* **2022**, *13*, 6853.

(20) Liu, X.; Jiao, Y.; Zheng, Y.; Jaroniec, M.; Qiao, S.-Z. Mechanism of C-N Bonds Formation in Electrocatalytic Urea Production Revealed by Ab Initio Molecular Dynamics Simulation. *Nat. Commun.* **2022**, *13*, 5471.

(21) Song, S.; Vuckovic, S.; Kim, Y.; Yu, H.; Sim, E.; Burke, K. Extending Density Functional Theory with Near Chemical Accuracy Beyond Pure Water. *Nat. Commun.* **2023**, *14*, 799.

(22) Huang, B.; von Rudorff, G. F.; von Lilienfeld, O. A. The Central Role of Density Functional Theory in the AI Age. *Science* **2023**, *381*, 170−175.

(23) Pandech, N.; Kongnok, T.; Palakawong, N.; Limpijumnong, S.; Lambrecht, W. R. L.; Jungthawan, S. Effects of the van der Waals Interactions on Structural and Electronic Properties of $CH_3NH_3(Pb,Sn)(I,Br,Cl)_3$ Halide Perovskites. *ACS omega* **2020**, *5*, 25723−25732.

(24) Rabiee, N.; Ahmadi, S.; Rabiee, M.; Bagherzadeh, M.; Vahabi, H.; Jouyandeh, M.; Saeb, M. R. Green carbon-based Nanocomposite Biomaterials through the Lens of Microscopes. *Emerg. Mater. Res.* **2022**, *5*, 665−671.

(25) Chen, B. W. J.; Xu, L.; Mavrikakis, M. Computational Methods in Heterogeneous Catalysis. *Chem. Rev.* **2021**, *121*, 1007−1048.

(26) Yuan, D.; Zhang, Y.; Ho, W.; Wu, R. Effects of van der Waals Dispersion Interactions in Density Functional Studies of Adsorption, Catalysis, and Tribology on Metals. *J. Phys. Chem. C* **2020**, *124*, 16926−16942.

(27) Li, J.; Wang, Y.; An, L.; Chen, J.; Yao, L. Direct Observation of CH/CH van der Waals Interactions in Proteins by NMR. *J. Am. Chem. Soc.* **2018**, *140*, 3194−3197.

(28) Stöhr, M.; Tkatchenko, A. Quantum mechanics of proteins in explicit water: The role of plasmon-like solute-solvent interactions. *Sci. Adv.* **2019**, *5*, No. eaax0024.

(29) Freire, R. L. H.; Guedes-Sobrinho, D.; Kiejna, A.; Da Silva, J. L. F. Comparison of the Performance of van der Waals Dispersion Functionals in the Description of Water and Ethanol on Transition Metal Surfaces. *J. Phys. Chem. C* **2018**, *122*, 1577−1588.

(30) Shirali, K.; Shelton, W. A.; Vekhter, I. Importance of van der Waals Interactions Forab Initiostudies of Topological Insulators. *J. Phys.: Condens. Matter* **2021**, *33*, 035702.

(31) Zhang, G.-X.; Tkatchenko, A.; Paier, J.; Appel, H.; Scheffler, M. Van der Waals interactions in ionic and semiconductor solids. *Phys. Rev. Lett.* **2011**, *107*, 245501.

(32) Yin, J.; Yang, H.; Song, K.; El-Zohry, A. M.; Han, Y.; Bakr, O. M.; Brédas, J.-L.; Mohammed, O. F. Point Defects and Green Emission in Zero-Dimensional Perovskites. *J. Phys. Chem. Lett.* **2018**, *9*, 5490−5495.

(33) Ferri, N.; DiStasio, R. A.; Ambrosetti, A.; Car, R.; Tkatchenko, A. Electronic properties of molecules and surfaces with a self-consistent interatomic van der Waals density functional. *Phys. Rev. Lett.* **2015**, *114*, 176802.
(34) Grimme, S. Semiempirical GGA-type Density Functional Constructed with a Long-range Dispersion Correction. *J. Comput. Chem.* **2006**, *27*, 1787−1799.
(35) Grimme, S.; Antony, J.; Ehrlich, S.; Krieg, H. A Consistent and Accurate Ab Initio Parametrization of Density Functional Dispersion Correction (DFT-D) for the 94 Elements H-Pu. *J. Chem. Phys.* **2010**, *132*, 154104.
(36) Tkatchenko, A.; Scheffler, M. Accurate Molecular van der Waals Interactions from Ground-state Electron Density and Free-atom Reference Data. *Phys. Rev. Lett.* **2009**, *102*, 73005.
(37) Bučko, T.; Lebègue, S.; Ángyán, J. G.; Hafner, J. Extending the applicability of the Tkatchenko-Scheffler dispersion correction via iterative Hirshfeld partitioning. *J. Chem. Phys.* **2014**, *141*, 34114.
(38) Tkatchenko, A.; DiStasio, R. A.; Car, R.; Scheffler, M. Accurate and Efficient Method for Many-body van der Waals Interactions. *Phys. Rev. Lett.* **2012**, *108*, 236402.
(39) Hermann, J.; Tkatchenko, A. Density functional model for van der Waals interactions: unifying many-body atomic approaches with nonlocal functionals. *Phys. Rev. Lett.* **2020**, *124*, 146401.
(40) Grimme, S.; Ehrlich, S.; Goerigk, L. Effect of the Damping Function in Dispersion Corrected Density Functional Theory. *J. Comput. Chem.* **2011**, *32*, 1456−1465.
(41) Reckien, W.; Janetzko, F.; Peintinger, M. F.; Bredow, T. Implementation of Empirical Dispersion Corrections to Density Functional Theory for Periodic Systems. *J. Comput. Chem.* **2012**, *33*, 2023−2031.
(42) Hirshfeld, F. L. Bonded-atom Fragments for Describing Molecular Charge Densities. *Theoret. Chim. Acta* **1977**, *44*, 129−138.
(43) Bultinck, P.; van Alsenoy, C.; Ayers, P. W.; Carbó-Dorca, R. Critical analysis and extension of the Hirshfeld atoms in molecules. *J. Chem. Phys.* **2007**, *126*, 144111.
(44) Vanpoucke, D. E. P.; Bultinck, P.; van Driessche, I. Extending Hirshfeld-I to bulk and periodic materials. *J. Comput. Chem.* **2013**, *34*, 405−417.
(45) Becker, M. A.; Vaxenburg, R.; Nedelcu, G.; Sercel, P. C.; Shabaev, A.; Mehl, M. J.; Michopoulos, J. G.; Lambrakos, S. G.; Bernstein, N.; Lyons, J. L.; Stöferle, T.; Mahrt, R. F.; Kovalenko, M. V.; Norris, D. J.; Rainò, G.; Efros, A. L. Bright Triplet Excitons in Caesium Lead Halide Perovskites. *Nature* **2018**, *553*, 189−193.
(46) Boziki, A.; Dar, M. I.; Jacopin, G.; Grätzel, M.; Rothlisberger, U. Molecular Origin of the Asymmetric Photoluminescence Spectra of $CsPbBr_3$ at Low Temperature. *J. Phys. Chem. Lett.* **2021**, *12*, 2699−2704.
(47) Mannino, G.; Deretzis, I.; Smecca, E.; La Magna, A.; Alberti, A.; Ceratti, D.; Cahen, D. Temperature-Dependent Optical Band Gap in $CsPbBr_3$, $MAPbBr_3$, and $FAPbBr_3$ Single Crystals. *J. Phys. Chem. Lett.* **2020**, *11*, 2490−2496.
(48) Beck, H.; Gehrmann, C.; Egger, D. A. Structure and Binding in Halide Perovskites: Analysis of Static and Dynamic Effects from Dispersion-corrected Density Functional Theory. *APL Mater.* **2019**, *7*, 21108.
(49) Latimer, K.; Dwaraknath, S.; Mathew, K.; Winston, D.; Persson, K. A. Evaluation of Thermodynamic Equations of State Across Chemistry and Structure in the Materials project. *NPJ. Comput. Mater.* **2018**, *4*, 40.
(50) Ghaithan, H. M.; Alahmed, Z. A.; Qaid, S. M. H.; Hezam, M.; Aldwayyan, A. S. Density Functional Study of Cubic, Tetragonal, and Orthorhombic $CsPbBr_3$ Perovskite. *ACS omega* **2020**, *5*, 7468−7480.
(51) López, C. A.; Abia, C.; Alvarez-Galván, M. C.; Hong, B.-K.; Martínez-Huerta, M. V.; Serrano-Sánchez, F.; Carrascoso, F.; Castellanos-Gómez, A.; Fernández-Díaz, M. T.; Alonso, J. A. Crystal Structure Features of $CsPbBr_3$ Perovskite Prepared by Mechano-chemical Synthesis. *ACS omega* **2020**, *5*, 5931−5938.
(52) Tammireddy, S.; Lintangpradipto, M. N.; Telschow, O.; Futscher, M. H.; Ehrler, B.; Bakr, O. M.; Vaynzof, Y.; Deibel, C. Hysteresis and Its Correlation to Ionic Defects in Perovskite Solar Cells. *J. Phys. Chem. Lett.* **2024**, *15*, 1363−1372.
(53) Kerner, R. A.; Rand, B. P. Ionic-Electronic Ambipolar Transport in Metal Halide Perovskites: Can Electronic Conductivity Limit Ionic Diffusion? *J. Phys. Chem. Lett.* **2018**, *9*, 132−137.
(54) Li, W.; She, Y.; Vasenko, A. S.; Prezhdo, O. V. Ab initio nonadiabatic molecular dynamics of charge carriers in metal halide perovskites. *Nanoscale* **2021**, *13*, 10239−10265.
(55) Agiorgousis, M. L.; Sun, Y. Y.; Zeng, H.; Zhang, S. Strong Covalency-Induced Recombination Centers in Perovskite Solar Cell Material $CH_3NH_3PbI_3$. *J. Am. Chem. Soc.* **2014**, *136*, 14570−14575.
(56) Li, W.; Sun, Y. Y.; Li, L.; Zhou, Z.; Tang, J.; Prezhdo, O. V. Control of Charge Recombination in Perovskites by Oxidation State of Halide Vacancy. *J. Am. Chem. Soc.* **2018**, *140*, 15753−15763.
(57) Xue, J.; Wang, R.; Yang, Y. The surface of halide perovskites from nano to bulk. *Nat. Rev. Mater.* **2020**, *5*, 809−827.
(58) Wang, Y.; Wu, T.; Barbaud, J.; Kong, W.; Cui, D.; Chen, H.; Yang, X.; Han, L. Stabilizing heterostructures of soft perovskite semiconductors. *Science* **2019**, *365*, 687−691.
(59) Brenes, R.; Eames, C.; Bulović, V.; Islam, M. S.; Stranks, S. D. The Impact of Atmosphere on the Local Luminescence Properties of Metal Halide Perovskite Grains. *Adv. Mater.* **2018**, *30*, No. e1706208.
(60) Shi, H.; Du, M. H. Shallow Halogen Vacancies in Halide Optoelectronic Materials. *Phys. Rev. B* **2014**, *90*, 174103.
(61) Ran, J.; Wang, B.; Wu, Y.; Liu, D.; Mora Perez, C.; Vasenko, A. S.; Prezhdo, O. V. Halide Vacancies Create No Charge Traps on Lead Halide Perovskite Surfaces but Can Generate Deep Traps in the Bulk. *J. Phys. Chem. Lett.* **2023**, *14*, 6028−6036.
(62) Wu, Y.; Liu, D.; Chu, W.; Wang, B.; Vasenko, A. S.; Prezhdo, O. V. Fluctuations at Metal Halide Perovskite Grain Boundaries Create Transient Trap States: Machine Learning Assisted Ab Initio Analysis. *ACS Appl. Mater. Interfaces* **2022**, *14*, 55753−55761.
(63) Chu, W.; Zheng, Q.; Prezhdo, O. V.; Zhao, J.; Saidi, W. A. Low-frequency Lattice Phonons in Halide Perovskites Explain High Defect Tolerance toward electron-hole recombination. *Sci. Adv.* **2020**, *6*, No. eaaw7453.
(64) Wang, B.; Chu, W.; Wu, Y.; Casanova, D.; Saidi, W. A.; Prezhdo, O. V. Electron-Volt Fluctuation of Defect Levels in Metal Halide Perovskites on a 100 ps Time Scale. *J. Phys. Chem. Lett.* **2022**, *13*, 5946−5952.
(65) Zheng, Q.; Chu, W.; Zhao, C.; Zhang, L.; Guo, H.; Wang, Y.; Jiang, X.; Zhao, J. Ab Initio Nonadiabatic Molecular Dynamics Investigations on the Excited Carriers in Condensed Matter Systems. *Wiley Interdiscip. Rev. Comput. Mol. Sci.* **2019**, *9*, No. e1411.

https://doi.org/10.1021/acs.jpclett.4c02390
J. Phys. Chem. Lett. 2024, 15, 10465−10472